Wavelength-specific reflections: A decade of extreme ultraviolet actinic mask inspection research

K. A. Goldberg[a] and I. Mochi
Lawrence Berkeley National Laboratory, Cyclotron Road, Berkeley, California 94720

(Received 9 July 2010; accepted 30 August 2010; published 18 November 2010)

Mask inspection is essential for the success of any pattern transfer lithography technology, and extreme ultraviolet lithography (EUVL), in particular, faces unique challenges. EUV masks' resonant-reflective multilayer coatings have a narrow, wavelength-specific response that dramatically affects the way that defects appear, *or disappear*, at various illuminating wavelengths. Furthermore, the ever-shrinking size of "critical" defects limits the potential effectiveness of deep ultraviolet inspection techniques over time. Researchers pursuing numerous ways of finding and characterizing defects on extreme ultraviolet (EUV) masks and have met with varying degrees of success. Their lessons inform the current, urgent exploration to select the most effective techniques for high-volume manufacturing. Ranging from basic research and demonstration experiments to commercial inspection tool prototypes, the authors survey the recent history of work in this area, including sixteen projects in Europe, Asia, and America. Solutions range from scanning beams to microscopy, darkfield imaging to pattern transfer. © *2010 American Vacuum Society.*
[DOI: 10.1116/1.3498757]

I. INTRODUCTION

Photomask defects are a potential stumbling block for any pattern transfer lithography. Finding, removing, and repairing defects are difficult yet essential steps for the economical creation and use of masks. The problem becomes more difficult as feature sizes shrink with every successive lithography generation. For extreme ultraviolet lithography (EUVL), which uses a much shorter light wavelength than preceding generations (13.5 versus 193 nm), the situation is acute, and mask *defectivity* has risen to become one of the highest concerns within the EUV lithography community.

EUV lithography presents specific challenges arising from the use of all-reflective optical elements, the wavelength-specific optical properties of materials, and among other issues, the current opinion that mask-protecting pellicles will not be compatible with EUV lithography.[1] Beginning in 1994, with the first EUV reflective masks[2] and with Motorola's creation of the first prototype full-field EUVL mask in 1999,[3] the race has been on to create high-quality, efficient mask inspection and imaging tools.

Most defects can be identified using existing or emerging non-EUV techniques. However, the unknown wavelength-specific optical properties of native defects, combined with the resonant-reflective response of multilayer mirrors, makes the prediction of EUV printing properties from non-EUV measurements a highly uncertain task. "Buried" substrate or interlayer particles, bumps, and pits that can distort the multilayer coating structure have been recognized as a serious concern from very early research in EUV lithography.[4] Such defects are often referred to as *phase defects* because of their effect on the reflected field of the aerial image. Owing to the resonant response of multilayer mirrors, non-EUV inspection methods may be largely insensitive to some classes of critical mask defects. It may also be true that non-EUV inspection methods can be oversensitive to defects that would not significantly disturb the EUV aerial image.

As we look to the future, with shrinking design rules and ever smaller critical defect sizes, the current consensus is that EUV lithography in high-volume manufacturing will require EUV actinic inspection and imaging tools,[5] in particular, for pattern sizes below 22 nm. Between now and then, opportunities exist with the current prototype tools to perform cross-calibration measurements to assess risk and understand the limits of non-EUV inspection.

Beginning in the mid-1990s, several groups separately demonstrated the importance of actinic mask inspection. In the intervening years, with more than a dozen different research projects by many of the world's leading EUVL research teams, there has been significant learning, but progress has often come slowly. Early work answered a pressing research question by demonstrating the presence of *actinic only* defects—defects that could only be detected with EUV light.[6] However, several years later, opinions were still divided about the presence or the significance of such defects. Now, in 2010, with numerous prototypes demonstrating the importance and feasibility of actinic inspection and imaging, at least one commercial supplier is stepping forward, creating a new generation of EUV actinic mask imaging tools.[7]

This article reviews current progress in the field of EUV actinic mask inspection and imaging, briefly describing the most significant, published projects during the past 13 years. Readers may also wish to consult Ref. 8, an earlier review paper that described several of the most significant actinic mask inspection projects in Japan and the United States in

[a]Electronic mail: KAGoldberg@lbl.gov

TABLE I. EUV actinic mask inspection and imaging projects.

Technique	Detection medium	Group	Year	References
Mask blank inspection				
Low-resolution scanning mask defect inspection	EUV	LBNL (EUV LLC)	1998	6, 12, and 13
Moderate-resolution scanning mask defect inspection	EUV	LLNL, LBNL, SEMATECH	2005	14–20
Defect decoration with photoresist coating	EUV, photoresist, visible light	BNL, Bell Laboratories	1998	21–24
All-EUV darkfield imaging with low-resolution	EUV	MIRAI	2003	25–29
All-EUV darkfield imaging with scanning	EUV	MIRAI/SELETE	2009	30–32
Static low and moderate resolution all-EUV darkfield imaging	EUV	Aachen University	2009	33–35
Photoelectron microscopy	EUV, electrons	University of Bielefeld	2006	36–39
High-resolution mask imaging				
EUV interferometric microscope with a high-magnification electron lens	EUV, electrons	NTT		40–43
EUV Schwarzschild microscope with a high-magnification electron lens	EUV, electrons	University of Hyogo	2003	8 and 43–48
Two-stage image magnification: EUV to visible	EUV, visible light	Exitech	2005	49 and 50
Synchrotron-based high-magnification EUV zoneplate imaging	EUV	LBNL/SEMATECH	2006	15 and 51–58
EUV zoneplate imaging with a broadband source	EUV	University of Albany, INVENT	2007	58–60
EUV zoneplate imaging with an EUV laser	EUV	Colorado State University	2009	61–64
EUV AIMS™ with a high-magnification reflective lens	EUV	Carl Zeiss	2012	7
Synchrotron-based coherent-scattering microscopy	EUV	University of Hyogo	2007	65–69
Multimode actinic inspection	EUV	Hanyang University	2010	70

more detail. The public record may be incomplete, and we offer our apologies to projects and research not known to us at the time of writing.

II. INSPECTION AND IMAGING

Mask inspection and imaging microscopy serve several distinct purposes that reflect the semiconductor and mask fabrication process. Excluding the inspection of printed wafers, these methods fall into at least three distinct categories: (1) blank inspection, (2) aerial image microscopy, and (3) high-speed pattern inspection. To date, actinic inspection and imaging research projects have focused on the first two categories, with pattern inspection viewed as the most challenging of all. One commonly shared opinion is that deep-ultraviolet mask blank inspection tools may be able to serve the needs of EUV lithography in high-volume manufacturing for the 22 nm node.[9,10] However, this opinion is not unanimous, and projections for working solutions beyond 22 nm are unreliable because experimental evidence is incomplete.

Aerial image microscopy, frequently referred to as "AIMS™ mode,"[11] is a technique used to predict a mask's imaging performance in a stepper (i.e., a lithographic printing tool) without printing into photoresist. Ideally, the illumination and imaging conditions replicate those of given stepper models. A high-magnification lens enables the recording of the aerial image intensity pattern reflected from the mask surface. Such tools do not cover large areas; they are used in a point-by-point inspection mode, often in concert with defect repair steps.

The third category of mask inspection is rapid scanning of a patterned mask to search for defects. The pattern imaging may be performed with a higher spatial resolution and different illumination conditions than the scanner since the goal is to rapidly identify defects that can be reviewed further using other methods. Among the most common methods for defect identification are (1) to record images for comparison with a detailed model, and (2) the direct imaging comparison of two nominally identical mask regions, measured simultaneously, in parallel. To date, no such actinic systems have been created or publicly disclosed.

A. Actinic inspection methodologies

To characterize the EUV optical response unambiguously, a mask must be illuminated with EUV light. This firm prerequisite is common to all-EUV actinic methodologies. Following EUV illumination, only our collective creativity and resourcefulness bound the variety of ways used to detect a mask's response.

Two main signal detection categories have emerged: light and photoemission. The dominant method is to detect the reflected EUV light. Imaging the EUV light requires the use of high-quality EUV optical systems, with or without a scintillator that converts EUV light to another detectable medium, e.g., visible-light or electrons. A smaller number of groups have focused on the detection of the directly ejected photoelectrons. Electron imaging systems can be built with high resolution, but such systems face the additional challenges of linearity and dynamic range. In all cases, detection efficiency is a critical success criterion, given the limited power and brightness or the restrictive cost of available EUV sources for metrology.

There are significant differences between systems designed to detect defects on blank masks and those designed to produce high-resolution images of defects and mask patterns. The projects described here are organized according to this distinction. Table I provides an overview of the various inspection techniques described in this article.

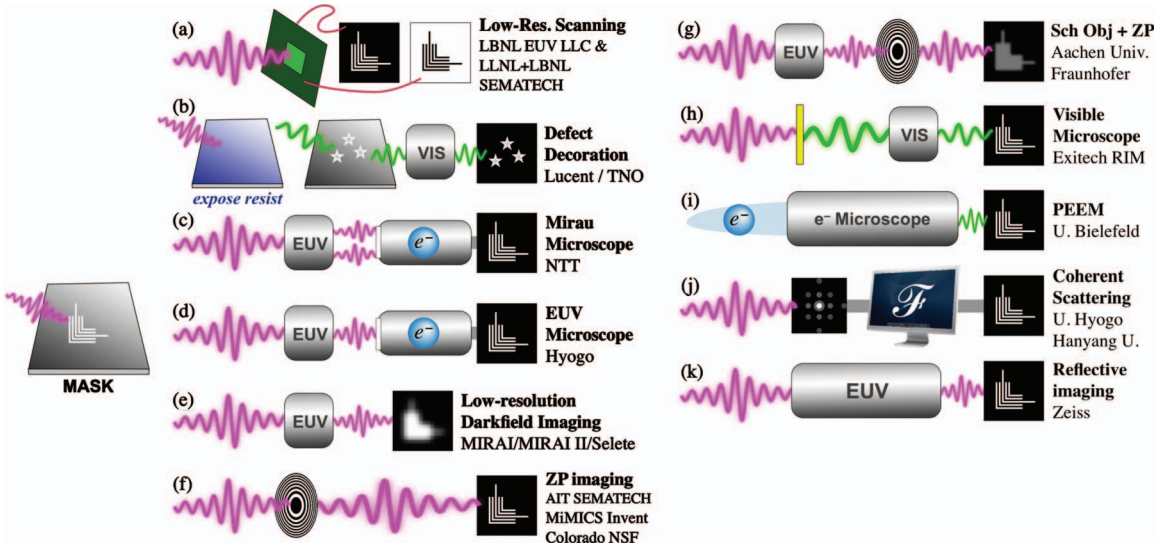

FIG. 1. (Color) Schematic depiction of the various actinic mask inspection techniques, arranged by category, roughly in the chronological order in which they came into operation. In each case, the mask is illuminated with EUV light. Some systems detect EUV photons directly [(a), (e), (f), (g), (j), and (k)], others detect photoelectrons [(c) and (d)] or convert the EUV or photoelectron image to visible-light [(b), (h), and (i)].

III. EUV ACTINIC MASK BLANK INSPECTION PROJECTS

Defects on blank masks can reduce the reflected light amplitude and scatter light out of the specular reflected beam. Among the first successful strategies used in actinic EUV mask inspection was detecting both the reflected brightfield (specular) and darkfield (scattered or diffracted) EUV light from a focused beam scanning across the mask surface. In this mode, the sensitivity to small defects in the brightfield channel relies on a relatively small beam size and a stable photon flux level. Put simply, an opaque 100 nm defect in a 1 μm beam absorbs only 1% of the reflected light; smaller defects become more difficult to detect in proportion to this area ratio. Given a target sensitivity to a particular defect size, instability in the photon flux level or noise in the detection electronics sets the maximum rate at which data can be collected at points across the mask surface.

Quantifying darkfield sensitivity is more complex. Relatively speaking, smaller defects scatter less light into wide solid angles. Therefore, darkfield sensitivity relies on large solid-angle coverage and sensitive detectors. Darkfield detection must exclude the specular, brightfield signal to isolate the small signals associated with defect scattering. Within a certain solid angle that is dependent on surface properties, a persistent background signal level is generated by scattering from the random surface roughness and multilayer phase roughness.

A. Scanning mask blank inspection

1. Low-resolution scanning mask defect inspection

Funded by the EUV LLC, the Bokor group at Lawrence Berkeley National Laboratory (LBNL) created the first actinic mask inspection system on a synchrotron bending-magnet beamline [Fig. 1(a)].[12] A Kirkpatrick–Baez (KB) mirror pair formed a fixed, focused beam on a vertically mounted mask that was raster-scanned in two dimensions. A Channeltron™ was positioned to record the brightfield reflected signal, while a microchannel plate measured the darkfield. The system was the first to unambiguously detect the presence of actinic only defects,[6,12] and by 2001 was able to detect buried defects as small as 30 nm wide and 3 nm tall at the top surface.[13]

Although it was limited to slow scan speeds, the LBNL tool was years ahead of its successors and demonstrated several *firsts*, including actinic observation of phase defects, native defects, and micron-scale mask roughness, and the characterization of darkfield defect diffraction patterns.

2. Moderate-resolution scanning mask defect inspection

A SEMATECH-funded successor to the Bokor group project utilized the same scanning principle, yet with a smaller, 1–5 μm focused beam, and a design intended to enable higher-speed mask scanning [Fig. 1(a)].[14] The *Berkeley actinic mask inspection tool*, as it was called, began operations in 2005.[15]

Using an idea first put forth in 2000 by Jeong *et al.*[16] to achieve the smaller focused spot size, Barty *et al.* placed a 20–100 μm pinhole in the focus of the KB. The pinhole was reimaged onto the mask with a 20× demagnification, and an illumination angle of 6° from normal, by an EUV Schwarzschild objective (SO), using an off-axis subaperture for an unobstructed pupil. The brightfield signal was detected using a photodiode, and the darkfield signal with an annular microchannel plate (MCP). The mask was mounted on an $x\theta z$ stage to provide high-speed through rotation.

As originally designed, a multilayer-coated turning mirror directed the reflected beam horizontally toward the detectors, from the small space between the SO and the mask. The limited angular bandpass of the turning mirror's multilayer

coating significantly reduced the collectable solid angle of the darkfield detector.[17] In addition, imperfections in the turning mirror increased the scattered light level, reducing the detection sensitivity.

In a 2006 revision, the brightfield and darkfield detectors were replaced with small photodiodes positioned side-by-side, facing the mask directly.[18] While the new photodiodes improved the brightfield performance, the low signal level and vibration-limited beam intensity stability reduced the speed and sensitivity. Goldberg *et al.* noted a trade-off between the sensitivity gains made possible by a small spot size and the decreased signal-to-noise ratio from the lower total flux that accompanied it. (A 2.5 μm beam spot was typically used for brightfield measurements.[18]) Low flux levels virtually eliminated the possibility of high-speed scanning.

Among the most significant results from the Berkeley actinic mask inspection tool was the further demonstration of the importance of both brightfield and darkfield detection modes.[19] Certain defects, in particular, micron-scale absorptive regions (due to surface contamination or multilayer coating damage) may not generate a measurable darkfield signal. Therefore, it was suggested that mask inspection techniques that rely solely on darkfield detection are potentially vulnerable to overlooking these defects entirely,[20] a point confirmed by other groups. Other measurements included the characterization of ultraviolet-laser-damage test regions with micron-scale spatial resolution. The measurements were sensitive to reflectivity variations as small as 0.5%.[18]

B. Defect decoration with photoresist coating

In 1998, Spector *et al.*,[21] with researchers from the Brookhaven National Laboratory, Bell Laboratories, and elsewhere, proposed to identify mask blank defects by finding changes to an exposed photoresist applied to the mask surface, or to a thin closely positioned membrane [Fig. 1(b)]. Using a well-controlled EUV flood exposure, defects on the resist-covered mask modulate the latent image in the resist and would thus be visible by optical inspection after development. Their work demonstrated that with the appropriate EUV dose and a high-contrast resist, defects as small as 1.8% intensity change could disrupt the reflected signal enough to print into the photoresist layer.[22]

One variation of the technique, demonstrated in 1999,[23] applied the photoresist not to the mask, but to a thin, EUV-transparent membrane brought into close proximity to the mask surface. The near-field diffraction pattern from a defect could locally affect the resist exposure, and the presence of a defect could be discovered. Defects as small as 200 nm were identified with this technique.

In 2010, 12 years after the method's initial description, a different group, Nijkerk *et al.*[24] proposed a re-evaluation of the method using state of the art inspection tools. Their simulations predict that the method is still worthy of consideration.

C. EUV darkfield imaging

Small mask blank defects (with sizes on the order of one to several EUV wavelengths) diffract light into relatively large solid angles where they can be detected by darkfield imaging. In darkfield imaging, the specular reflected beam is blocked and usually discarded, while an image is formed from the available scattered or diffracted light. Its main advantage is a significant improvement in the detection's signal-to-noise ratio relative to brightfield. Darkfield systems sacrifice high resolution for the potentials of high speed and sensitivity. Three darkfield mask imaging systems have been created, with very similar configurations, described here.

1. All-EUV darkfield imaging with low-resolution

Researchers from MIRAI (Japan) developed a mask blank inspection system based on low-resolution, darkfield imaging with all-EUV magnification and detection [Fig. 1(e)]. Their system first described in detail in 2003 (Refs. 25 and 26) used a standalone laser-produced plasma (LPP) light source and demonstrated successful measurements of programed-defect array masks in 2004.[27,28]

In the MIRAI tool, light from the LPP is collected by a large area ellipsoidal mirror and focused onto the mask surface at normal incidence using a small turning mirror close to the mask surface. The reflected light is magnified 20× and projected onto an EUV charge coupled device (CCD) camera by an on-axis SO. The annular collection angle of the SO had a maximum numerical aperture (NA) value corresponding to 0.2 and an inner, obscured NA value of 0.1. This annular collection solid angle effectively blocks the specular light and most of the scattered intensity from multilayer and substrate roughness, leaving only the darkfield signal (e.g., from defects) for image formation. The obscured central solid angle also potentially blocks diffraction from defects above 50–100 nm diameters. Tezuka *et al.*[26] predicted that larger (converging) illumination solid angles (up to 8°) significantly improve the collection efficiency for defects above this size, while noting that such defects could also be detected using available nonactinic inspection tools.

In 2004, with a source operating at 10 Hz, The MIRAI tool could record statistically good static images of a 0.5×0.5 mm^2 region of the mask with a 10 s exposure. Tezuka *et al.* extrapolated from their measured source power (2.4×10^{10} photos or 3.6×10^{-7} J/pulse) to determine that the energy required to cover 142×142 mm^2 of a mask surface is 2.9 J. Therefore, in order to reach a rate of 1 h per mask, the authors calculated the EUV illumination power on the mask surface would be 2 mW—a large, but not unreasonable value considering the EUV power required by steppers. The speed-limiting factor in this static imaging configuration is the CCD readout rate. At 1 MHz, data-readout would consume 12 h for a whole mask. (This issue would be addressed by a successor project, the MIRAI-SELETE tool.)

An upgrade to the MIRAI tool, referred to as MIRAI II, gave the imaging system a higher magnification SO (26×) and a larger darkfield collection solid angle, ranging from

0.20 to 0.26 NA.[29] At this magnification, the effective square pixel size corresponds to a 500 nm region of the mask. The upgraded tool had sensitivity to defects 1.5 nm high and 60 nm wide, measured at the top surface of the multilayer, yet its performance suffered from optical aberrations resulting from alignment errors in the SO.

2. All-EUV darkfield imaging with a scanning mask

The SELETE tool [Fig. 1(e)] is based on the MIRAI II tool, but uses scanning mask stages and continuous CCD readout (*Time Delay and Integration*) to achieve dramatically higher inspection rates.[30,31] The 26× SO was aligned and achieved clear, high-quality imaging. Yamane *et al.*[30] reported that the signal-to-noise ratio for darkfield defect detection decreased with increasing scanning speed, forcing them to raise the detection threshold and thereby lose sensitivity. In early 2010, improvements in focus control and signal processing to minimize CCD noise were being investigated.

The darkfield scanning approach to blank mask inspection, may have some application in patterned mask inspection as well. In their most recent report, Terasawa *et al.*[32] demonstrated how their darkfield scanning tool can detect the presence of defects within highly regular patterns.

3. Static low and moderate resolutions all-EUV darkfield imaging

Recently, a group lead by Juschkin of the Rheinich-Westfälische Technische Hochschule Aachen University (Germany) has begun collecting data with a moderately high-magnification all-EUV mask imaging system that combines a SO with a zoneplate lens for two magnification stages [Fig. 1(g)].[33,34] Their system is installed at the Fraunhofer Institute for Laser Technology and is powered by an AIXUV GmbH xenon-based gas discharge EUV source. With a relatively simple configuration, their goal is to create an efficient standalone inspection prototype and investigate its sensitivity for darkfield blank mask defect detection.

As a proof of principle, the system was operated successfully with a transmission mask. A ring ellipsoid collector creates an annular illumination pattern at normal incidence on the mask. An on-axis SO with an annular pupil and a NA value of 0.22 projects the image with a 21.34× magnification. With the addition or removal of a central beam-stop ahead of the SO, the single-stage magnification system can be used as a brightfield or a darkfield microscope, focusing onto the CCD plane. In a second configuration, the authors introduced a zoneplate lens to project the intermediate image created by the SO onto a CCD camera with an additional 10–20× magnification. The annular zoneplate used in this configuration has a focal length of 3.2 mm, a low object-side NA value of 0.011, and thus requires only 30 zones, a good bandwidth match for the illumination. Initial results with the transmission masks show the detection of darkfield features as small as 100 nm and isolated bright dots with 500 nm diameter and spacing, with some significant issues in scattered or background light and transmission from unblocked zoneplate orders.[33,34] Herbert *et al.*[35] described recent successful mask measurements performed in the reflective geometry, without the zoneplate. This configuration resembles the original MIRAI geometry with static detection. The authors report a detection of absorbing defects as small as 40 nm, and bump defects down to 250 nm with the potential for higher sensitivity with increased flux density.

D. Photoelectron microscopy

Photoelectron microscopy offers a different approach to actinic mask inspection and imaging. Using high-resolution electron lenses removes the challenge of creating tightly focused EUV beams and imaging. In 2006, Kleineberg and co-workers[36,37] from the University of Bielefeld (Germany), and others, developed a photoemission electron microscope (PEEM) to image the EUV field amplitude at the mask surface with high-resolution [Fig. 1(i)]. The sensitive correlation between the photoemission and the EUV reflective properties of multilayer mirrors (including phase) arises from the EUV standing wave and the field intensity near the surface, as discussed by Miyake *et al.*[38] Lin *et al.* demonstrated blank inspection and pattern imaging with the PEEM microscope.

In the Bielefeld EUV-PEEM, a modified, commercially available instrument (Focus GmbH, Germany), photoelectrons and secondary electrons emitted from the surface of a mask are projected onto a MCP for amplification onto a fluorescent screen. A CCD camera connected to the screen records the PEEM image. The tool uses a toroidal multilayer mirror to concentrate EUV light from a synchrotron undulator beamline onto a 100 μm mask area with a 4° angle of incidence, allowing subsecond exposure times. The PEEM field of view could be varied from 1 mm down to 2.3 μm in seconds. The authors measured a spatial resolution limit of 29 nm, yet later describe 50–100 nm as typical.[39]

As expected from the standing wave, the observed image contrast reverses as the incident light wavelength is tuned across the multilayer coating's Bragg peak.[38] Unexpected results include wide buried lines appearing as mere contours and of narrow lines as appearing significantly wider than expected. Lin *et al.* attributed the broadening to the buried defect's depth (below the multilayer)—at which the phase disturbance originates—being outside of the narrow depth of focus. The images are also affected by nonuniformity and localized dark defects in the scintillator. In 2008, Lin *et al.* described a method of "interference contrast" in which they tuned the illuminating wavelength to a photoemission minimum and thereby highlighted the appearance of the standing-wave-disturbing defects. The sensitivity enhancement is analogous to darkfield scattering measurements in the scanning-beam or low-resolution imaging tools.[40]

IV. HIGH-RESOLUTION EUV ACTINIC MASK IMAGING PROJECTS

While mask blank inspection focuses on speed and sensitivity, high-resolution imaging serves a broader purpose. Measuring the continuous intensity distribution reflected from a mask enables predictive modeling of lithographic per-

formance, along with a deeper understanding of the severity of various defects, the effectiveness of defect mitigation strategies, the quantitative evaluation of various mask architectures, and optical proximity corrections, among other uses.

Among the many projects in this category, groups have employed several different methods to achieve a high magnification: the need to magnify nanometer-scale mask features up to micron-size detector pixels drives the design.

High-quality zoneplate lenses are well known in short-wavelength microscopy applications. Their simplicity and potential for very high-magnification ratios is counterbalanced by their requirement for narrow-bandwidth illumination and their potentially small, aberration-minimized field of view.

Low-magnification (10–30×) reflective EUV lenses have been used for more than 20 years. Applying them to high-resolution mask imaging requires coupling their output to an additional magnification stage, whether by scintillator conversion to visible light or photoelectrons, or with an additional EUV lens. High-magnification EUV reflective optics have only recently been deemed feasible.[7] In all cases, EUV reflective optical systems for this purpose must be created to diffraction-limited quality, with system wavefront errors limited to a small fraction of the EUV wavelength (i.e., below 1 nm). This is a significant and expensive challenge for surface figuring, multilayer coating, optical housing stability, and for interferometric testing, whether performed with visible-light, EUV light, or both.

Coherent diffraction imaging (CDI) is an emerging method that eliminates lenses altogether, reconstructing the mask surface field over a small region based on recorded diffraction patterns. By avoiding the limitations of zoneplates and the potential cost and challenge of reflective optics, CDI trades simplicity in the experimental configuration for complexity and uncertainty in the image reconstruction.

A. EUV interferometric microscope with a high-magnification electron lens

The Mirau interferometric microscope (MIM), demonstrated by Haga *et al.*[40] of Nippon telegraph and telephone (NTT), was the first high-resolution actinic imaging microscope for EUV mask research. Described in 2000, the microscope illuminated the mask surface through one subaperture of a 15× SO and imaged the mask through the other [Fig. 1(c)]. The synchrotron-based tool projected an image using two magnification stages, with conversion from a low-magnification EUV stage to a high-magnification electron lens. An x-ray zooming tube employed a CsI photocathode as an x-ray imaging plate, and variable-magnification electron optics (from 10–200×, giving a total system magnification from 150–3000×), to record the images.

The Mirau concept uses a freestanding multilayer beam splitter[41] parallel to the mask surface to split the incident light. The transmitted beam is reflected from the mask surface and passes back through the beamsplitter. The reflected beam serves as a reference: it bounces away from the mask to a reference flat multilayer mirror positioned facing the mask and equidistant from the mask. When the reference beam again reflects from the beamsplitter, it interferes with the first beam, enabling the phase-properties of the mask to be sensitively probed. Focusing is achieved by an independent adjustment of the mask and reference mirrors' longitudinal positions. Phase and amplitude defects can be separately identified by their behavior as the focal position of the reference mirror is tuned: phase defects show a unique signature of contrast changes not present with amplitude defects.

In Mirau interferometric mode, the microscope demonstrated a resolution of 800 nm dense lines for absorptive and phase-shifting patterns, and sensitivity to native and programed defects with step heights as small as 5 nm. In 2003, the same system was used as a prototype for the EUV microscope (EUVM) developed by Kinoshita and co-workers.[42,43] In the latter work, the microscope clearly resolved dense absorber line patterns as small as 250 nm. Furthermore, by direct comparison with scanning electron microscopy (SEM), Haga *et al.* showed that some defects clearly observed in the SEM would not significantly affect the EUV images. Such early work underscored the importance of actinic mask imaging for accurate defect detection.

B. EUV Schwarzschild microscope with a high-magnification electron lens

The EUVM developed by Kinoshita *et al.* at the University of Hyogo (formerly Himeji Institute of Technology) is the successor to the early NTT work of Haga *et al.* [Fig. 1(d)].[4] Operating on a bending magnet beamline at the New SUBARU synchrotron radiation facility, EUVM demonstrated high-resolution imaging and the detection of buried phase defects.[44]

The EUVM design is similar to the MIM, illuminating the mask though a subaperture of a SO, and then using a two-stage magnification system.[44] A low-magnification, 30× EUV SO (using an off-axis subaperture or the full-aperture with a beam-splitter[45]), projects an image onto the entrance scintillator of a 10–200× x-ray zooming tube; the total system magnification therefore ranges from 300–6000×.

A number of published studies show that the EUVM clearly detects defects buried below the multilayer coating.[8,44,46–48] Line defects as small as 90 nm wide and 4 nm tall, or 100 nm wide and 2 nm tall (at the substrate) have been observed.

As with other EUV imaging tools, the EUVM faces significant challenges achieving illumination (and detector) uniformity and reaching diffraction-limited performance from the objective lens.

C. Two-stage image magnification: EUV to visible

In 2005, Booth *et al.*[49] reported Exitech's (United Kingdom) extensive research and development effort to create the first commercial EUV actinic mask inspection microscope, the RIM-13. The microscope used a two-stage magnification system with conversion from EUV to visible-light for image

detection [Fig. 1(h)]. Two separate subapertures of a single high-NA optic served as both the final stage of the condenser and the EUV objective. With a 10× magnification and 0.0625 NA, the imaging subaperture projects the magnified mask image onto a thin, single-crystal of Ce-doped yttrium aluminum garnet for conversion to visible-light. From the scintillator, a wide-field variable-magnification microscope objective system relayed the 540 nm wavelength image onto a low-noise CCD camera detector. The complete system had magnification values of 250, 500, or 750×. While the RIM-13 design was optimized for a source with 10–50 μm sizes, early trials were conducted with a 400 μm source supplied by AIXUV GmbH.[50]

Ultimately, problems and delays beset the project and Exitech declared bankruptcy weeks to months before the RIM-13 tools were delivered. It could be argued that Exitech's collapse in 2006 stole significant momentum from progress in (and funding for) actinic mask inspection efforts for several years.

D. High-magnification all-EUV imaging with a zoneplate objective

Zoneplate objectives are attractive as prototype mask imaging tools for their single-optical-element simplicity. Zoneplates operate by diffraction; to avoid chromatic aberrations, they require narrow-band illumination. This aspect alone makes high-magnification zoneplates generally unsuitable for use with broadband EUV light sources. They can be produced with high accuracy by electron-beam lithography, or possibly by nanoimprint lithography, for greater cost savings. To date, three groups have pursued high-magnification zoneplate microscope designs.

1. Synchrotron-based high-magnification EUV zoneplate imaging

The SEMATECH mask inspection tool, described previously, is a dual-mode microscope. In addition to scanning-beam inspection mode, the original system also incorporated an off-axis, high-magnification Fresnel zoneplate lens with 0.0625 NA to image the mask surface [Figs. 1(a) and 1(f)].[15] Initially (2005–2007), the system was beset by significant deficiencies in zoneplate-positioning control, illumination nonuniformity, and high vibration.

With numerous upgrades to the system, Goldberg *et al.* made significant advances and refinements in the zoneplate lens approach,[51,52] and renamed the tool the *SEMATECH Berkeley Actinic Inspection Tool* (AIT). The AIT is the first zoneplate microscope to incorporate an array of user-selectable objective lenses with different optical properties. Five lenses had 4× NA values from 0.25 to 0.35, giving the AIT higher spatial resolution than existing printing tools, and magnification up to 1000×, for an effective mask pixel size as small as 13.5 nm in the images. By 2007–2008, the mask images showed dramatic improvement and the AIT became a reliable user facility. With greater illumination uniformity from mirror scanning, and improved imaging from zoneplate engineering and quantitative fine alignment feedback,[53] the AIT was used in a series of benchmarking tests to fully characterize its performance.[51,52] Flare, which had been a concern since its inception, was demonstrated to be relatively low, between 2% and 3%, using a modified version of Kirk's method.[54] The measured contrast transfer function is above 50%, for dense lines as small as 70 nm. Coherence measurements revealed a partial coherence σ value below 0.2 (a value much lower than anticipated by its designers). The AIT overcomes mask and zoneplate stage limitations and records stable through-focus image series using a wavelength-tuning approach that utilizes the zoneplate's chromatic focal length dependence.[55]

Despite its slow speed (typically 45 s per image), a vibration quenching mechanism that requires touching the mask surface, and a lack of kinematic mask positioning (which makes navigation challenging), the AIT is currently the highest performing actinic mask imaging tool. It is used in native and patterned defect studies[56,57] of both blank and patterned masks, and it is routinely used in the study of mask architectures, contamination,[58] multilayer phase roughness, and defect repair, among other topics.

2. EUV zoneplate imaging with a broadband source

In 2007, Denbeaux *et al.*[59] at the College of Nanoscale Science and Engineering in Albany (US), funded by the INVENT consortium, developed a standalone zoneplane microscope called the *Microscope for Mask Imaging and Contamination Studies* (MiMICS). MiMICS uses an EUV light source from Energetiq Technology, Inc. (Woburn, MA). To narrow the broad spectrum, the system used a transmission filter, reflection from a multilayer-coated mirror, and a zoneplate condenser lens to illuminate the mask surface. Similar to the AIT, an off-axis zoneplate objective lens was designed to project a high-magnification image onto an EUV CCD camera [Fig. 1(f)].

Various difficulties, including the inadequate filtering of non-EUV light, prevented the recording of EUV images. Work with the MiMICS tool reverted to mask (carbon) contamination studies,[58] including the strong dependence of contamination rates on out-of-band radiation.[60]

3. EUV zoneplate imaging with an EUV laser

Tabletop EUV laser sources[61] have recently been proposed as a candidate for standalone EUV metrology tools. The plasma-based, collisional laser demonstrated by Colorado State University (Fort Collins, CO) operates at 13.2 nm wavelength, within the bandpass of typical EUV multilayer mirrors, and delivers narrowband illumination ($\Delta\lambda/\lambda < 1 \times 10^{-4}$) that is suitable for use with zoneplate lenses. The EUV laser has sufficient power (several microwatts) to record high-quality images in 1–2 min, operating at 1 Hz.

Brizuela *et al.*[62,63] created a compact zoneplate microscope prototype that has been successfully used in high-resolution mask imaging [Fig. 1(f)]. Somewhat similar to the design of MiMICS, their system uses a multilayer-coated turning mirror and a condenser zoneplate to illuminate a small field of view, at a 6° incidence with a partial coherence

σ of approximately 0.25.[64] Similar to the AIT, an off-axis zoneplate with 0.0625 NA projects the image of the illuminated mask directly onto an EUV CCD camera with 660× magnification. As with other imaging tool prototypes, illumination uniformity has been challenging to achieve.

While the Colorado Group showed clearly patterns with feature sizes as small as 80 nm half-pitch, the authors claim a spatial resolution limit of 55 nm based on independent image sharpness metrics they developed.[63]

E. EUV AIMS™ with a high-magnification reflective objective

Amid growing anxiety within the EUV lithography community about the unavailability of commercial actinic mask imaging tools, Carl Zeiss recently announced a highly sophisticated EUV AIMS™ (aerial image microscope system) project planned for delivery in late 2013 [Fig. 1(k)].[7]

The proposed all-EUV optical imaging system uses a standalone source, and is projected to deliver 1 s exposure times using a 10 μm square image region. Partial coherence is freely controlled using various aperture plates. The illumination chief ray angle is adjustable from 6° to 9° for work above 0.35 NA (wafer-side 4× equivalent). Furthermore, to accurately emulate the ring-field imaging conditions in a stepper, the chief ray is capable of rotating azimuthally while measuring various points across the mask.

One significant and novel aspect of the Zeiss design is an all-reflective microscope objective with 750× magnification. To achieve a reasonable, 1 m track length, the lens has four mirrors: one asphere and three spherical elements. The final element has extremely challenging specifications with a beam footprint of only 120 μm diameter and a requirement for rms roughness below 35 pm. While similar EUV lenses have never been created before, Feldmann *et al.*[7] reported that the required surface smoothness levels have already been demonstrated.

F. Coherent scattering microscopy

Coherent scattering microscopy (CSM), also known as CDI, and informally as *lensless imaging*, is an unconventional idea that has garnered great interest in the x-ray and synchrotron communities.[65,66] The concept is appealingly simple: Illuminate a small region of a mask with coherent light and directly record the pattern of scattered and diffracted light using a CCD detector (no lens is used). In principle, the complex-valued electric field reflected from the mask (i.e., both amplitude and phase information) can be reconstructed uniquely from the far-field pattern. Doing so eliminates the cost and complexity of having an EUV objective lens and eliminates the aberrations that track their use. Furthermore, it offers the opportunity to mathematically predict the entire through-focus image series (process window, etc.) from the single complex field reconstruction.

1. Synchrotron-based coherent-scattering microscopy

Lead by Kinoshita *et al.*[67] the group from the University of Hyogo, working at the New SUBARU synchrotron light source, created the first successful CSM tool for EUV masks [Fig. 1(j)]. Their work demonstrated the utility and simplicity of CSM for the measurement of mask pattern features, especially critical dimension (CD). Using the New SUBARU system, researchers from Samsung performed horizontal-vertical (h-v) bias studies of patterns with different absorber layer thicknesses; the data compared favorably with the SEMATECH Berkeley microfield-exposure tool.[68]

Because of the relatively simple detector geometry, the measurement solid angle can be increased (thereby improving the potential spatial resolution in the reconstruction) by bringing the detector closer to the mask. Once the diffraction pattern has been recorded, arbitrary stepper NA values and coherence properties can be emulated mathematically by filtering, manipulating, and recombining the raw data. The limitation of CSM may be its relative insensitivity to small isolated defects. Small defects scatter weakly, and their diffraction pattern can cover the entire detector area. Unlike conventional imaging where a point defect's light is focused into a small region of the image, CSM image reconstruction must extract the weak defect signal from among the stronger signals created by the pattern elements. Accurate reconstruction therefore requires very high signal-to-noise ratio and a high dynamic range detector.

The Kinoshita group is also developing a new CSM system using a tabletop high-order harmonic generation laser EUV source.[69]

2. Hanyang University

Led by Professor Ahn, a group at the Hanyang University (Korea) is developing multimode EUV metrology systems using a synchrotron source.[70] Their systems include the capabilities for CSM [Fig. 1(j)], reflectometry, and aerial image measurement. In Spring 2010, they demonstrated CSM operations with an angular range large enough to measure the CD of 50 nm dense lines on the mask.

V. CONCLUSION

While it seems that many in the semiconductor industry are just now coming to the realization that EUV actinic inspection and imaging tools will be required to meet the stringent demands of high-volume manufacturing (HVM) at 22 or 16 nm nodes, several groups of pioneers have been leading work in this field since the late 1990s.

Among the projects designed for early learning, for basic research, and as commercial tools and prototypes, there have been at least 15 separate EUV actinic mask inspection and imaging projects undertaken to date. Ultimately mask inspection may require a combination of EUV and non-EUV tools or inspection modes.

Mask inspection, the search for defects on mask blanks, has largely settled on low-resolution darkfield imaging with direct EUV detection. The MIRAI and MIRAI II projects

achieved the greatest sensitivity and speed for static exposures with a standalone source. If the scanning signal-to-noise ratio issues can be resolved, it is our opinion that the MIRAI II-SELETE project currently holds the greatest promise in this area.

For high-resolution mask imaging, all-EUV zoneplate microscopes based on a synchrotron or an EUV laser source have achieved the greatest degree of success to date. Research from the SEMATECH-funded AIT at LBNL has produced valuable data in every area of mask imaging. With improvements in laser power, Colorado State University's tabletop zoneplate microscope may point the way to practical, standalone, aerial image microscopes.

Systems that utilize a low-magnification EUV lens, with image conversion to electrons or visible-light, cannot escape the critical requirements associated with producing and aligning EUV optics with diffraction-limited wavefront quality. Excitech's unfortunate and expensive failure to deliver the first commercial EUV mask imaging tools likely stole considerable momentum from the drive to commercialize EUV lithography.

In 2010, Zeiss' entry into the field, with a high-magnification all-reflective EUV optical system design scheduled for delivery in late 2013, has renewed confidence for many, that commercial solutions will become available in time for HVM. Yet Zeiss' goals and tool specifications are very aggressive. In our opinion, the major players would be wise to mitigate risk by funding additional, ongoing and emerging research projects. Clearly, there remains room for innovations, and tool designs can evolve as source power levels improve over time.

EUV's at-wavelength measurement requirements may be different than those of the previous lithography generations. Specialized solutions such as CSM may find niche application in CD measurement and other qualifications.

As HVM approaches and anxiety grows, the EUVL community now appears to recognize the urgency of continued research and funding in the critical area of EUV actinic mask inspection and imaging.

ACKNOWLEDGMENTS

The authors gratefully acknowledge the support of SEMATECH, and researchers such as Obert Wood, Stefan Wurm and others within the SEMATECH member companies who have been strong proponents of actinic mask inspection and imaging. The authors are indebted to the many researchers in this area, for their groundbreaking work, and for sharing their thoughts and publications lists with them. They include Hiroo Kinoshita, Jeffrey Bokor, Seongtae Jeong, Chris Walton, Scott Hector, Steve Spector, Yoshihiro Tezuka, Tsuneo Terasawa, Greg Denbeaux, Jinho Ahn, Chang Young Jeong, Bruno LaFontaine, Ulf Kleineberg, Wolfgang Harnisch, Tetsuo Harada, Larissa Juschkin, and their research teams. Special thanks are also due to Vivek Bakshi who suggested this review project. This work is funded by SEMATECH under Project No. LITH-343S2 and was performed under the auspices of the U.S. Department of Energy by the University of California Lawrence Berkeley National Laboratory under Contract No. DE-AC02-05CH11231.

[1]H. Meiling *et al.*, Proc. SPIE **7271**, 727102 (2009).
[2]D. M. Tennant *et al.*, J. Vac. Sci. Technol. B **9**, 3176 (1991).
[3]Business Wire, Tuesday, 3 August 1999.
[4]K. B. Nguyen, T. Mizota, T. Haga, H. Kinoshita, and D. T. Attwood, J. Vac. Sci. Technol. B **12**, 3833 (1994).
[5]B. Rice, EUVL Symposium 2009, Prague, Czech Republic, October 21, 2009 (unpublished).
[6]M. Yi, T. Haga, C. Walton, C. Larson, and J. Bokor, Jpn. J. Appl. Phys., Part 1 **41**, 4101 (2002).
[7]H. Feldmann, J. Ruoff, W. Harnisch, and W. Kaiser, Proc. SPIE **7636**, 76361C (2010).
[8]H. Kinoshita, K. Hamamoto, N. Sakaya, M. Hosoya, and T. Watanabe, Jpn. J. Appl. Phys., Part 1 **46**, 6113 (2007).
[9]D. Wack, Q. Q. Zhang, G. Inderhees, and D. Lopez, Proc. SPIE **7636**, 76360V (2010).
[10]P. Gargini, (ITRS, SIA), EUVL Symposium 2009, Prague, Czech Republic, October 21, 2009 (unpublished).
[11]AIMS is a trademark of Carl Zeiss SMT AG.
[12]S. Jeong *et al.*, J. Vac. Sci. Technol. B **16**, 3430 (1998).
[13]M. Yi, T. Haga, C. Walton, and J. Bokor, J. Vac. Sci. Technol. B **19**, 2401 (2001).
[14]Y. Liu, A. Barty, E. Gullikson, J. S. Taylor, J. A. Liddle, and O. Wood, Proc. SPIE **5751**, 660 (2005).
[15]A. Barty, Y. Liu, E. Gullikson, J. S. Taylor, and O. Wood, Proc. SPIE **5751**, 651 (2005).
[16]S. Jeong, C.-W. Lai, S. Rekawa, C. C. Walton, and J. Bokor, Proc. SPIE **3997**, 431 (2000).
[17]K. A. Goldberg, EIPBN 2006, see http://goldberg.lbl.gov/presentations/p2/EIPBN_2006/
[18]K. A. Goldberg, S. B. Rekawa, C. D. Kemp, A. Barty, E. H. Anderson, P. Kearney, and H. Han, Proc. SPIE **6921**, 69213U (2008).
[19]A prediction noted in Ref. 6.
[20]K. A. Goldberg, A. Barty, P. Seidel, K. Edinger, R. Fettig, P. Kearney, H. Han, and O. R. Wood II, Proc. SPIE **6517**, 65170C (2007).
[21]S. J. Spector, D. L. White, D. M. Tennant, P. Luo, and O. R. Wood II, Proc. SPIE **3546**, 548 (1998).
[22]S. J. Spector, P. Luo, A. E. Novembre, L. Ocola, D. L. White, D. M. Tenant, and O. R. Wood II, Proc. SPIE **3676**, 606 (1999).
[23]S. J. Spector, D. L. White, D. M. Tennant, L. E. Ocola, A. E. Novembre, M. L. Peabody, and O. R. Wood II, J. Vac. Sci. Technol. B **17**, 3003 (1999).
[24]D. Nijkerk, N. Koster, E. van Brug, and D. Maas, Proc. SPIE **7636**, 763622 (2010).
[25]T. Tomie, T. Terasawa, Y. Tezuka, and M. Ito, Proc. SPIE **5038**, 41 (2003).
[26]Y. Tezuka, M. Ito, T. Terasawa, and T. Tomie, Proc. SPIE **5038**, 866 (2003).
[27]Y. Tezuka, M. Ito, T. Terasawa, and T. Tomie, Proc. SPIE **5374**, 271 (2004).
[28]Y. Tezuka, T. Terasawa, M. Ito, and T. Tomie, Proc. SPIE **5446**, 804 (2004).
[29]T. Yamane, T. Iwasaki, T. Tanaka, T. Terasawa, O. Suga, and T. Tomie, Proc. SPIE **7122**, 7122D (2008).
[30]T. Yamane, T. Iwasaki, T. Tanaka, T. Terasawa, O. Suga, and T. Tomie, Proc. SPIE **7271**, 72713H (2009).
[31]T. Terasawa, T. Yamane, T. Tanaka, T. Iwasaki, O. Suga, and T. Tomie, Jpn. J. Appl. Phys., Part 1 **48**, 06FA04 (2009).
[32]T. Terasawa, T. Yamane, T. Tanaka, O. Suga, T. Kamo, and I. Mori, Proc. SPIE **7636**, 763602 (2010).
[33]L. Juschkin, R. Freiberger, and K. Bergmann, J. Phys.: Conf. Ser. **186**, 012030 (2009).
[34]L. Juschkin and R. Freiberger, Proc. SPIE **7360**, 736005 (2009).
[35]S. Herbert, A. Maryasov, L. Juschkin, R. Lebert, and K. Bergmann, Proc. SPIE **7545**, 75450O (2010).
[36]U. Kleineberg *et al.*, Proc. SPIE **6151**, 615120 (2006).
[37]J. Lin *et al.*, J. Vac. Sci. Technol. B **24**, 2631 (2006).
[38]A. Miyake, M. Amemiya, F. Masaki, and Y. Watanabe, J. Vac. Sci. Tech-

nol. B **22**, 2970 (2004).
[39]J. Lin, N. Weber, M. Escher, J. Maul, H.-S. Han, M. Merkel, S. Wurm G. Schönhense, and U. Kleineberg, Opt. Express **16**, 15343 (2008).
[40]T. Haga, H. Takenaka, and M. Fukuda, J. Vac. Sci. Technol. B **18**, 2916 (2000).
[41]T. Haga, M. C. K. Tinone, M. Shimada, T. Ohkubo, and A. Ozawa, J. Synchrotron Radiat. **5**, 690 (1998).
[42]T. Haga, H. Kinoshita, K. Hamamoto, S. Takada, N. Kazui, S. Kakunai, H. Tsubakino, and T. Watanabe, Jpn. J. Appl. Phys., Part 1 **42**, 3771, (2003).
[43]H. Kinoshita *et al.*, J. Vac. Sci. Technol. B **22**, 264 (2004).
[44]K. Hamamoto Y. Tanaka, S. Y. Lee, N. Hosokawa, N. Sakaya, M. Hosoya, T. Shoki, T. Watanabe, and H. Kinoshita, J. Vac. Sci. Technol. B **23**, 2852 (2005).
[45]M. Osugi, K. Tanaka, N. Sakaya, K. Hamamoto, T. Watanabe, and H. Kinoshita, Jpn. J. Appl. Phys., Part 1 **47**, 4872 (2008).
[46]K. Hamamoto *et al.*, Proc. SPIE **6151**, 615119 (2006).
[47]H. Kinoshita, K. Hamamoto, N. Sakaya, M. Hosoya, T. Shoki, Y. Mizuta, T. Yoshizumi, K. Tanaka, and T. Watanabe, Microelectron. Eng. **84**, 1015 (2007).
[48]K. A. Goldberg, K. Takase, P. Naulleau, H. Han, A. Barty, H. Kinoshita, and K. Hamamoto, SPIE Advanced Lithography 2008, see http://goldberg.lbl.gov/presentations/p2/SPIE_2008B/.
[49]M. Booth *et al.*, Proc. SPIE **5751**, 78 (2005).
[50]R. Lebert *et al.*, Proc. SPIE **5374**, 943 (2004).
[51]K. A. Goldberg *et al.*, Proc. SPIE **6730**, 67305E (2007).
[52]K. A. Goldberg, I. Mochi, P. P. Naulleau, H.-S. Han, and S. Huh, Proc. SPIE **7122**, 71222E (2008).
[53]I. Mochi, K. A. Goldberg, P. Naulleau, and S. Huh, Proc. SPIE **7271**, 76361A (2009).
[54]J. P. Kirk, Proc. SPIE **2197**, 566 (1994).
[55]K. A. Goldberg, I. Mochi, and S. Huh, Proc. SPIE **7271**, 72713N (2009).
[56]S. Huh *et al.*, Proc. SPIE **7636**, 76360K (2010).
[57]I. Mochi, K. A. Goldberg, B. M. LaFontaine, A. Tchikoulaeva, and C. Holfeld, Proc. SPIE **7636**, 7636A (2010).
[58]Y.-J. Fan *et al.*, Proc. SPIE **7636**, 76360G (2010).
[59]G. Denbeaux *et al.*, EUVL Symposium 2007, Sapporo, Japan October 31, 2007 (unpublished); see http://www.sematech.org/meetings/archives/litho/8059/pres/ME-02-Denbeaux.pdf.
[60]G. Denbeaux, P. Thomas, Y.-J. Fan, A. Antohe, L. Yankulin, R. Garg, A. Wüest, and V. Jindal, Workshop on Surface Science Related to EUV Optics Contamination, NIST, Gaithersburg, MD, 2 June 2009 (unpublished).
[61]J. J. Rocca, Y. Wang, M. A. Larotonda, B. M. Luther, M. Berrill, and D. Alessi, Opt. Lett. **30**, 2581 (2005).
[62]F. Brizuela *et al.*, Opt. Lett. **34**, 271 (2009).
[63]F. Brizuela *et al.*, Proc. SPIE **7271**, 72713F (2009).
[64]F. Brizuela (personal communication).
[65]J. Miao, P. Charalambous, J. Kirz, and D. Sayre, Nature (London) **400**, 342 (1999).
[66]S. Marchesini *et al.*, Opt. Express **11**, 2344 (2003).
[67]T. Harada, J. Kishimoto, T. Watanabe, H. Kinoshita, and D. G. Lee, J. Vac. Sci. Technol. B **27**, 3203 (2009).
[68]H.-S. Seo *et al.*, J. Vac. Sci. Technol. B **26**, 2208 (2008).
[69]E. J. Takahashi, Y. Nabekawa, and K. Midorikawa, Appl. Phys. Lett. **84**, 4 (2004).
[70]J. Ahn and C. Jeong (private communication).